Strain-induced changes to the methanation reaction on thin-film nickel catalysts

Journal:	*Catalysis Science & Technology*
Manuscript ID	CY-ART-04-2019-000735
Article Type:	Paper
Date Submitted by the Author:	17-Apr-2019
Complete List of Authors:	Johnson, Benjamin; Brown University, School of Engineering Guduru, Pradeep; Brown University, Engineering Department Peterson, Andrew; Brown University, School of Engineering

Strain-induced changes to the methanation reaction on thin-film nickel catalysts

Benjamin Johnson, Pradeep R. Guduru, Andrew A. Peterson

School of Engineering, Brown University, Providence, RI 02906 USA

May 23, 2019

Abstract

We investigate how mechanical strain can directly manipulate the catalytic rate of a purely thermochemical reaction. Specifically, this work applies strain to a nickel-based thin film catalyst used in carbon monoxide methanation, which can serve as a key step in obtaining useful hydrocarbon fuels from biomass lignin. Previous computational literature has suggested that the application of mechanical strain can increase the activity of nickel-based catalysts in this reaction, making them a more attractive low-cost alternative to other more active catalysts. To directly apply strain in a high-temperature reactor, we designed a novel two-cell reactor which allowed us to use static air pressure to create a strained thin-film catalyst, ultimately measuring strain-induced changes in catalyst activity. In contrast with earlier theoretical predictions, increased tensile strain caused a decrease in activity rather than the increase which was originally expected. A re-examination of the computational reaction data suggests that the reaction model previously employed, which used a single parameter (CO dissociation energy) to predict catalyst activity, was overly simplified. It is likely that hydrogenation reaction steps have some rate-determining behavior and should be incorporated into the reaction model.

1 Background

Many catalytic reactions are best carried out over rare and expensive catalyst materials, making it difficult to implement these reactions economically at a large scale. This problem can potentially be addressed through modification of low-cost materials to increase their activity for certain reactions and make them a more attractive substitute. Interestingly, the chemical and catalytic properties of metals can, under the proper conditions, be altered solely through mechanical influences such as tensile or compressive strain. The fundamentals of this can be explained in either an electronic [1] or mechanical [2] framework, but in either case is manifested through a change in binding strength of reactive intermediates. In typical scenarios, strain is induced directly in the synthesis of the catalyst. For example, if a nanoparticle of one metal is enclosed in a thin layer of a different metal, their differing lattice parameters create a strain on the outside layer, as described in Wu *et al.* [3]. Such materials often have a coupled strain and "ligand" effect, where the latter effect describes the changes in the surface atoms due to having different chemical neighbors at differing strain levels, as an artifact of the preparation. While these effects can readily be separated computationally [4], it is challenging to unambiguously measure strain affects (separate from ligand effects) experimentally.

Recently, a number of electrochemical studies [5] [6] [7] [8] [9] have employed mechanical strain in order to cleanly and directly assess the impact of strain on surface reactivity. Such electrocatalytic

studies have some distinct advantages: the reaction can be carried out at room temperature and differences in reactivity with strain can be directly measured via shifts in the electrical potential of the reaction (for example, at a specified current density). For example, Yan *et al.* [8] developed a specialized reactor in order to examine the effect of external strain. A metallic catalyst deposited on a polymer substrate was secured in a mechanical strain testing machine while also enclosed in an electrochemical cell, enabling the study of the hydrogen evolution reaction while simultaneously varying the tensile or compressive uniaxial strain in the catalyst. Interestingly, the study was repeated for different characteristic metals, and different directional results were observed depending on whether the metal binds hydrogen too strongly or too weakly relative to the ideal catalyst, in agreement with the "volcano plot" picture of the hydrogen evolution reaction.

However, to our knowledge there have been no direct measurements of strain effects in conventional heterogeneous catalysis. These systems exhibit additional challenges over the electrocatalytic analogs. First, such reactions typically operate at elevated temperatures, so such a test system must be capable of holding strain at high temperatures. Second, the reaction rate must be measured via the careful measurement of reaction products (as opposed to simple voltage or current measurements available in electrochemical systems). Because all direct-strain setups employed to date have limited surface area, this poses a challenge in producing a great enough quantity and concentration of products to detect changes caused by strain.

A recent computational study [10] explores the effect of biaxial strain on stepped Ni(211), observing that CO causes a significant deformation when binding on top of the step. This system was suggested to exhibit unexpected behavior in response to strain due to the presence of a large mechanical component, relative to the traditional effects predicted from the changing electronic structure. However, the normal electronic effects are stronger for separate C$*$ and O$*$ adsorbates. As a result, this study finds that the application of strain has an unusually large effect on the dissociation energy for CO splitting, which has been previously correlated to overall activity for the CO methanation reaction.

The significance of this finding is that it can potentially increase the viability of Ni as a catalyst for methanation (Eqn. 1). Ru in particular is known to be more active for methanation than Ni but also significantly more expensive. Francis and Curtin suggest that with the application of approximately 3% biaxial strain, the activity of Ni could increase to rival that of Ru. The main objective of the present study is to experimentally examine this theory. After constructing a reactor that can conduct thermochemical methanation on both strained and unstrained Ni catalysts, it should be possible to compare their relative activities towards the conversion of CO to CH_4 and compare the results with those predicted by the theory.

$$CO + 3H_2 \longrightarrow CH_4 + H_2O \tag{1}$$

To our knowledge, no published study has directly measured the influence of mechanical strain on the reactivity of a catalyst in a purely thermochemical (*i.e.*, not electrochemical) reactor. Such a system would have several advantageous qualities, the most important of which is the degree of control one has over the observed strain on the catalyst which allows for unambiguous measurements of the strain effect. Strain generation from core-shell particles, dopants, and similar methods requires manufacturing precision to obtain a desired level of strain, which is fixed at the time of synthesis and cannot be altered; thus, strain effects are strongly coupled to ligand effects and cannot be disambiguated. In contrast, an external force can be controlled, easily measured, and changed during reactor operation.

However, several design challenges must be addressed in order to operate a reactor whose catalyst can be subjected to external forces to create strain. Our approach, described in detail in

the following section, is inspired by that used in the electrocatalytic study of Yan *et al.* with a thin-film catalyst on a flexible substrate. That study created strain through the use of a mechanical linear testing machine. This approach proved to be effective but requires that the reactor is built and operated near this machine. In the current setup we use static air pressure on the opposite side of the substrate in order to induce strain in the thin film. This approach requires smaller, less complicated equipment to implement, which allows for greater flexibility in reactor design and operation. The present study will demonstrate how this methodology can be used to directly measure strain effects in this reaction.

Other complications arise in the measurement of strain effects in a thermocatalytic, as opposed to electrocatalytic setup, most notably in thermal stability and product analysis. First, thermocatalytic reactions require high operating temperatures—as opposed to the room-temperature electrocatalytic reactions employed in earlier studies—which creates challenges for the material stability. Second, the measurement of the rate of reaction in electrocatalytic studies is relatively simple, as one just monitors the electrical current, and small changes can be detected. In the current setup, we must rely on the analysis of the gas-phase products exiting the reactor, which is challenging due to the small surface areas that we can achieve in strained film catalysts. Our strategies for overcoming these challenges are discussed in the following.

2 Experimental Methods

2.1 Reactor Design and Construction

Three factors were critical in guiding the initial reactor design steps. The reactor needed to be capable of carrying out methanation on strained and unstrained active Ni catalysts; it should be small enough to operate in a standard chemical hood to minimize the safety risk posed by the use of CO; and the design should have some level of flexibility so that the process can be modified as necessary based on initial results.

Mechanical strain was applied using a two-cell reactor design illustrated in Figure 1. A thin Ni film is deposited on a flexible substrate that is fixed between the two cells. One cell serves as the reactor and has the reactant gas flowing through it, while the other cell can be pressurized, flexing the substrate and creating strain on the substrate. The Ni film is thin enough that it inherits the strain and material properties of the substrate while retaining the catalytic and chemical properties of the Ni film.

Polyether ether ketone (PEEK) was chosen as the substrate and was obtained in sheets with thickness 0.030 in. (CS Hyde Co.) One of several commercially available 'high-performance' thermoplastics, PEEK has a high tensile strength and operating temperature. It is also readily available commercially at a thickness which, based on initial calculations discussed in depth in Section 3.2, gives a significant but not excessive strain response when subjected to pressures of up to 60 psi. PEEK was also chosen over thin metallic foil substrates. Compared to polymer substrates, metals would allow a higher operating temperature but generally have lower elastic strain limits and require greater pressures to achieve comparable strain.

The reactor was constructed predominantly of carbon steel; stainless steel was avoided since its Ni content may provide background catalytic activity. The reactor was built around a pair of commercially available steel pipe flanges with a 6 in. outer diameter (OD). One flange was carbon steel with a NPT size 2 threaded pipe fitting (actual diameter of 2.375 in.) and served as the reaction cell. The other flange was stainless steel with a NPT size 1 threaded pipe fitting and was the pressure cell. The smaller fitting size required fewer adapter to connect to the pressurized air source, allowing for a smaller overall reactor. This specific part was not available in carbon steel,

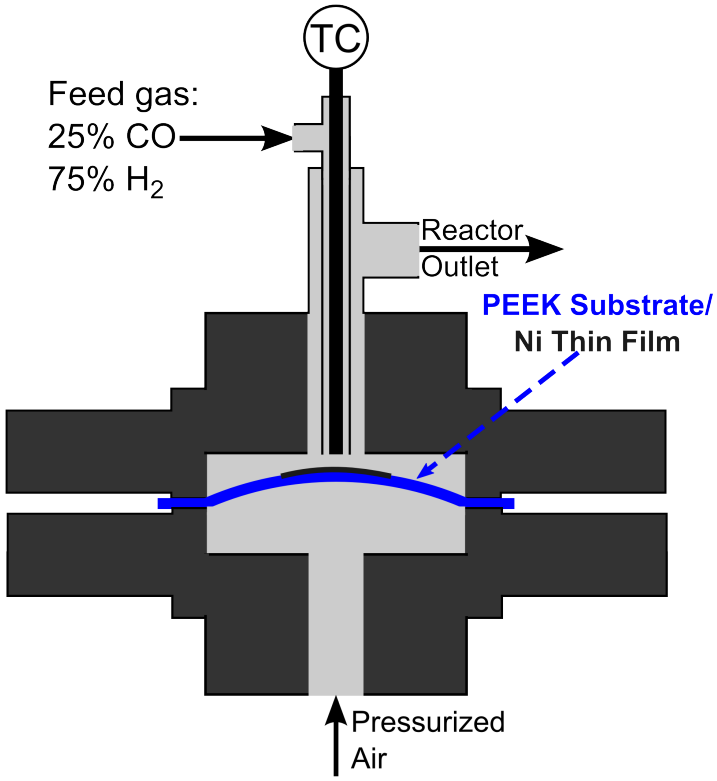

Figure 1: Cross-section schematic of methanation reactor (not to scale).

but it does not contact the feed gas and therefore does not introduce any background Ni catalytic activity. The catalyst substrates were fixed between the two flanges along with a compressible PTFE ring gasket to ensure an airtight seal between the flanges.

Threaded steel reducing pipe bushings were employed to convert the flange pipe fittings to NPT size 0.5, which allows for smaller and more convenient fittings to be attached to the flanges while retaining a large internal space to serve as the reaction cell. The reactor inlet and outlet streams flowed through nested concentric tubes with 0.25 in. and 0.5 in. ODs, respectively. This single nested inlet/outlet helps reduce the reactor size, minimizes the number of threaded connections needed, and concentrates flow in the center of the reaction cell where the catalyst is deposited. A 0.125 in. diameter thermocouple was also nested inside the inlet tube to monitor reactor temperature near the catalyst surface. Connections were made with standard compression tube fittings where possible, and a high-temperature silicone sealant (Permatex) was used on all NPT fittings to ensure an airtight seal.

Heat to the reactor was supplied using a heat cable controlled by a Watlow temperature controller and a thermocouple attached to the outside of the reactor. The heat tape and thermocouple were held in place using a high-temperature fiberglass-silicone adhesive tape. During operation, the reactor was wrapped in several layers of fiberglass insulation which improved heat retention, increased the uniformity of temperature throughout the system, and reduced the hazard posed by high-temperature reactor surfaces.

2.2 Product Analysis

Reactor outflow was analyzed sequentially by infrared spectroscopy (IR) and gas chromatography (GC). IR spectroscopy was performed on an Infrared Industries IR-208. The instrument was equipped to detect CO and CH_4 at concentrations up to 5000 ppm. Software supplied by the manufacturer was used to record CO and CH_4 concentrations at a frequency of 12 min^{-1}. This instrument proved to be effective for rapidly measuring CO concentrations, which are necessary to determine when steady state is reached and calculate a carbon balance. However, preliminary tests showed that CH_4 yield from the reactor was very low. CH_4 is known to be a poor IR absorber, and the amount of CH_4 generated was too low and resulted in an unacceptable signal-to-noise ratio. Therefore, GC was also used for product analysis. All reactor outlet gas flowed through the IR analytical chamber, and a tee fitting and needle valve then diverted part of the flow to the GC.

GC was performed on an Agilent 7890B gas chromatograph equipped with HayeSep Q and MolSieve 13X columns, thermal conductivity detector (TCD), and flame ionization detector (FID). The sampling program used was: injection at 65°C, hold for 1 minute, ramp 10°C/min for 5 minutes, and hold at 115°C for 1 minute. An air-actuated valve on the unit allowed for automated gas sampling. Gases continually flowed through the valve, and a 1 mL sample of gas was automatically injected after the previous run was completed and the oven had returned to its starting temperature. The GC FID provided superior sensitivity and accuracy in measuring CH_4 production. However, the available instrument could not effectively measure CH_4 and CO simultaneously without significant reconfiguration. As a result, both IR and GC analysis were necessary.

2.3 Computational Methodology

Computational analysis of the CO methanation reaction was conducted in order to gain a more complete understanding of the experimental results and their implications. Molecular simulation was carried out using Atomic Simulation Environment (ASE) with the Dacapo planewave density functional theory calculator for determining electronic structures. [11] Both are open-source software packages available from the Department of Physics at the Technical University of Denmark.

The catalyst surface was modeled as a $3 \times 3 \times 3$ atom cell of Ni atoms in a (211) configuration with the bottom two layers frozen. The unit cell employed periodic boundary conditions in all directions and 12 Å of vacuum between parallel Ni layers (resulting in a minimum of 10 Å vacuum when adsorbates were present). A dipole correction was also employed in the unit cell. The Ni cell and lattice parameter were optimized and used for adsorbate calculations on an unstrained surface. To simulate strained surfaces, the unit cell size was increased by the desired percent of strain and all atoms were subsequently allowed to relax without adsorbates to generate an optimized strained surface. This surface was then used in corresponding adsorbate calculations (with the bottom two layers frozen in their new positions.) This was done for strain values from 0 to 3 %, which reflects the levels of strain examined in Francis and Curtin.

DFT calculations were performed in spin-polarized mode using the RPBE exchange correlation functional [12], a plane-wave cutoff of 340.15 eV, and a density cutoff of 500.00 eV. A $4 \times 4 \times 1$ k-point sampling grid and Fermi temperature of 0.1 eV were utilized. Gas-phase calculations of CO, CH_4, and H_2 used Γ-point sampling and a Fermi temperature of 0.01 eV and were carried out in a $15.0 \times 15.1 \times 15.2$ Å cell.

Optimization of geometric structures was carried out using the BFGS line search algorithm [13], converging to a maximum force of 0.05 eV/Å. For each adsorbate, a separate optimization was carried out for each plausible initial configuration. After all optimizations were converged, the lowest energy configuration among them was assumed as the global optimum for that group

of adsorbates. Zero-point energies and free-energy contributions were then calculated for that adsorbate using standard statistical mechanical methods. Adsorbate calculations utilized harmonic approximations, while gas-phase species used the ideal gas approximation. Both cases assumed atmospheric pressure and a temperature of 250°C, matching the conditions of the experimental reactor.

A complete barrier calculation for every step of the reaction on every different strained surface would have required a substantial amount of computational resources. Instead, energy barriers were estimated using available scaling relation data in Wang *et al.* [14] [15] and Andersson *et al.* [16]. Vibrational modes for hydrogenation transition states were assumed to be the same as for the corresponding hydrogenated intermediate but with one less mode. The highest energy mode, which is associated with stretching the C−H bond that is eventually broken, was the discarded mode. Free energy corrections for transition states could then be estimated from the remaining modes using standard statistical mechanics.

These scaling relations give the transition state as a function of the binding energy of some related intermediate. Since the binding energies for all relevant intermediates were computed for Ni surfaces with varying levels of strain, barriers could easily be re-calculated for increasing strain levels by simply using a different binding energy corresponding to the strained surface.

It should be noted that this approach, along with much of the previous computational work regarding CO dissociation, focuses on step sites for the reaction. Experimentally, one would expect the catalyst used to be composed predominantly of planar facets such as (111) or (110) and that step sites such as (211) would be relatively scarce. However, Bengaard *et al.* [17] found DFT energies for CO dissociation over both Ni(111) and Ni(211) and predicts the activation energy to be greater on the (111) surface by approximately 90 kJ/mol. With such a difference in activation energies, and at a temperature of 250°C, the (211) site would be more reactive by a factor of over 9×10^8. It is therefore reasonable to assume that the reaction rate is driven entirely by step sites even if they are vastly outnumbered by planar sites.

3 Results and Discussion

3.1 Substrate Characterization and Reactor Parameters

The use of a thin film catalyst on a flexible substrate allows mechanical strain to be directly applied to the catalyst without a convoluting ligand effect. However, a drawback to this approach is that the active surface area is limited to the two-dimensional substrate face. Conventional packed-bed reactors employ a three-dimensional layer of powdered catalyst and support material around which reactants flow. The two-dimensional surface used here has significantly less active surface area and a correspondingly lower single-pass conversion rate. As a result, process operating parameters needed to be selected to maximize conversion and ensure that methane production was high enough to be accurately measured.

The first key operating parameter considered is temperature. Increased temperature should improve single-pass conversion but may also damage parts of the reactor and reduce the accuracy of product analysis. To optimize temperature, the reactor was loaded with a blank PEEK substrate and fed a stream of pure Ar. The reactor was initially heated to 200°C, and the temperature was increased by 10°C per hour while the reactor outflow was measured. At temperatures above 250°C, significant readings were observed on GC analysis, presumably due to offgassing from either the PEEK substrate or the silicone sealant. Therefore, the reactor was operated at 250°C to minimize this potential source of interference.

While material information on PEEK is available from the substrate vendor, this data is generally obtained at room temperature. Separate measurements were conducted to provide better data on the relationship between pressure and strain at elevated temperature. Strain measurements were accomplished using a fiber-optic displacement probe (Philtec muDMS-D169-C1T9) which measures and records the distance between the probe and a target surface. It was not practical to measure substrate displacement and strain *in situ*. Therefore, a separate set of tests was carried out using a blank substrate loaded in the reactor. The inlet tube was removed for this test to allow for the probe to better target the substrate. The modified reactor and probe were placed in an oven and heated to 250 °C. Pressure was then applied to the substrate, and the fiber-optic probe recorded the resulting change in substrate position. Corresponding strain was then calculated based on Equations 2 and 3:

$$\varepsilon_{measured} = \frac{L - 2r}{2r} \tag{2}$$

$$L = \left(\frac{r^2 + D^2}{D}\right) \sin^{-1}\left(\frac{2rD}{r^2 + D^2}\right) \tag{3}$$

Here, D is the measured displacement and r is the radius of the substrate disc (2.375 in.) This formula is derived by approximating the bulge in the substrate as part of a sphere, whose radius can be determined to be $\frac{r^2+D^2}{2D}$. The arc length of the spherical section, internal angle, and strain can then be found using straightforward geometry. The results of this testing are summarized in Table 1. At the highest pressure level tested, the substrate was under slightly less than 0.5% strain.

Applied pressure (psi)	Displacement (inch)	Strain
0	0	0%
5	0.0663	0.19%
10	0.0771	0.28%
15	0.0872	0.36%
20	0.0982	0.46%

Table 1: Strain level as a function of applied pressure

The reactor feed gas employed was a mixture of 25% CO and 75% H_2 (TechAir), which is the stoichiometric ratio required by Eqn. 1. Operating at a higher H_2:CO ratio would be expected to increase the fractional single-pass conversion of CO but would also dilute the total carbon in the stream, potentially making detection and measurement more difficult by lowering the overall concentration of CO and CH_4 below instrument detection limits. After preliminary testing, a feed rate of 2 standard cubic centimeters per minute (sccm) was chosen. This value was shown to give a reasonable balance between conversion rate and run time. Reactor feed gas flow was controlled using an Alicat MC-2SCCM-TFT/5M mass flow controller. The reactor output was mixed with a make-up gas stream of 100 sccm Ar, maintained using an Omega FMA-2617 mass flow controller. This increased the flow of the product stream to the analytical instruments and lowered run times. Under these conditions, experiments reached steady state within 2 hours.

3.2 Catalyst Fabrication

Thin film Ni was applied to the substrate via e-beam deposition conducted on a Kurt J. Lesker Lab 18 system. A 20 nm layer of Ni was deposited. Preliminary testing showed that the Ni adhered

well to the substrate without the need for a separate adhesion layer. To prevent oxidation, catalyst substrates were stored in an inert glove box until use.

For a flexible round disc under uniform pressure, strain is not uniform across the surface. Elastic deformation for this type of system has been studied extensively; strain is at a maximum at the center of the disc and decreases proportionally to the square of the distance from the center. Preliminary testing indicated that the substrates underwent both elastic and inelastic deformation, so the equations for elastic strain do not perfectly predict the present substrate behavior. However, based on the models for elastic deformation, it was decided that the Ni film would be deposited only on a small circular area, with a diameter of 0.61 in., in the center of the substrate disc. Strain within this area is expected to be no less than 80% of the maximum strain value on the substrate. This was chosen as an acceptable balance between allowing for a sufficiently large catalyst surface area while maintaining some level of uniformity in strain.

To prevent variance caused by minor differences in catalyst synthesis or surface properties, a single catalyst substrate was used for multiple experimental runs. Before each run, the catalyst was treated to ensure that all adsorbates were removed and that the catalyst was initially in the same state for each run. While at the target reaction temperature, the catalyst surface was reduced with 2 sccm H_2 for 2 hours. The reactor was then purged with 2 sccm Ar for a minimum of 1 hour to remove excess hydrogen from the system, with GC analysis used to verify that the reactor was purged of H_2.

3.3 Strain Methanation Experiments

Experiments were carried out at applied pressures of 0–20 psi in 5 psi increments, which resulted in the strain levels tabulated in Table 1. For each strain value, the experimental procedure was carried out three times. The same catalyst substrate was used for each test and was regenerated as described in Section 3.2. Tests at lower pressures were completed before proceeding to higher pressures. Due to the high temperature, some of the deformation applied on the substrate was plastic rather than elastic and was not completely reversible. Therefore, going from low to high pressure ensured better accuracy in the measured levels of strain.

Results of the methanation reactor tests are shown in Figures 2 and 3. These show, respectively, the absolute concentration of CH_4 in the reactor product stream and the percent of carbon conversion (concentration of CH_4 divided by combined concentrations of CH_4 and CO). Error bars in these figures indicate 95% confidence intervals.

Surprisingly, the data indicate that positive strain on the catalyst results in *decreased* CH_4 production and that catalyst activity was reduced, not increased as was originally predicted. Both concentration and percent conversion clearly decrease when going from 0% to 0.28% strain. The decline in activity is slower but still observable for tests at higher strains. Overall, the data shows that activity decreases by approximately 25% when catalyst strain is increased from 0% to 0.5%. This clearly does not support the theory proposed in [10], which suggests that this level of strain should cause an *increase* in activity of approximately 25%.

3.4 Computational Methanation Analysis

To better understand the apparent discrepancy between these experimental results and the proposed theory, the computational model used to predict methanation catalyst activity was revisited. The previous analysis, which serves as a foundation for the present work, focused heavily on the energy changes and barriers associated with the hydrogenation steps necessary to convert dissociated C^* and O^* adsorbates to CH_4 and H_2O products. Crucially, the prior work (which includes Francis

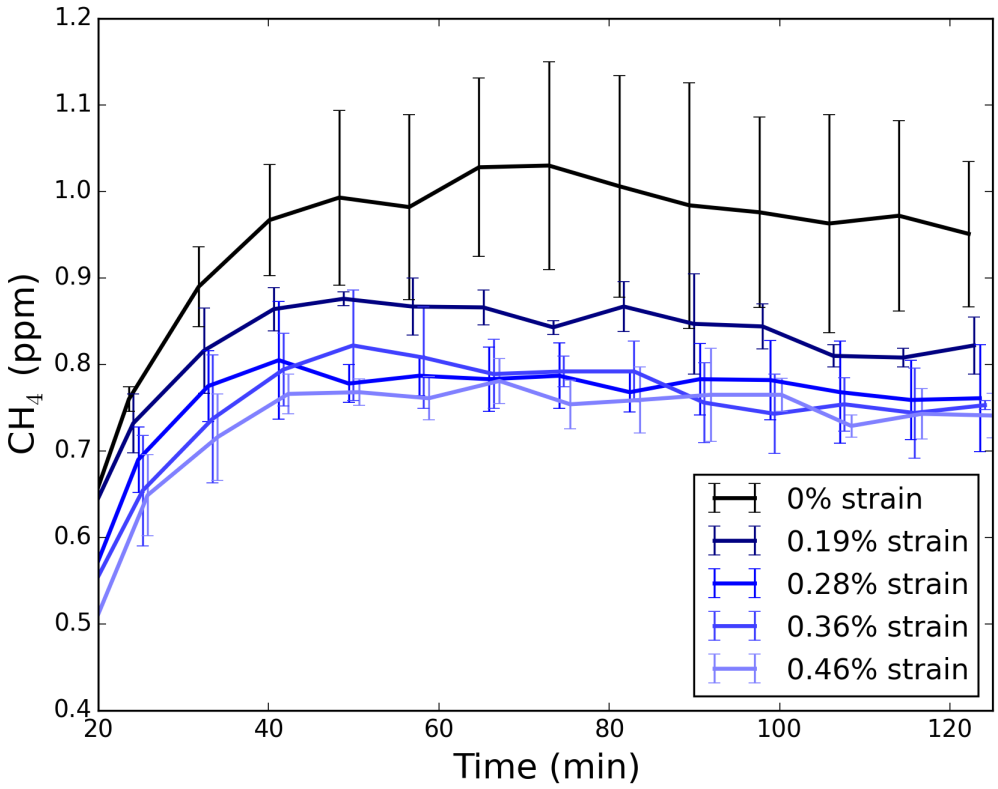

Figure 2: CH_4 concentrations and 95% confidence intervals

and Curtin [10], Andersson *et al.* [18], and Bligaard *et al.* [19]) focused on CO dissociation as the rate-determining step in the methanation reaction and made experimental measurements using a feed gas of 1% CO in H_2. Such conditions would encourage hydrogenation, discourage the formation of hydrocarbons heavier than CH_4, and allow researchers to better probe effects on CO dissociation. This approach was reasonable given the intended scope of those studies and the fact that the calculated barrier for CO dissociation is much greater than that of any hydrogenation step. However, it may also result in all hydrogenation steps occurring much faster than CO dissociation, and as a result it may obscure any rate-determining behavior of hydrogenation in the reaction.

The resulting energy diagram from these calculations is provided as Figure 4, which shows the results for all strain levels examined and normalized to one molecule each of CH_4 and H_2O. Here, we examined a wider strain range than in the experiments to be comparable to the work of Francis and Curtin [10]. The numerical data is also provided as Tables 2 and 3. This data shows that increased tensile strength results in weaker CO^* binding and a reduction in the CO dissociation barrier, which matches what is proposed by Francis and Curtin. However, increased tensile strength also results in larger barriers for the subsequent hydrogenation steps. The change for any one hydrogenation step is less than that observed for CO dissociation. However, the reaction requires six hydrogenation steps versus only one dissociation step, which can magnify even relatively small increases in hydrogenation barriers.

Of course, a coverage-dependent microkinetic model would be best capable of comparing the relative rates of different parts of the pathway. However, to simply compare these relative effects, in Table 4 the overall barriers are collected into two groups; that is, dissociation followed by hy-

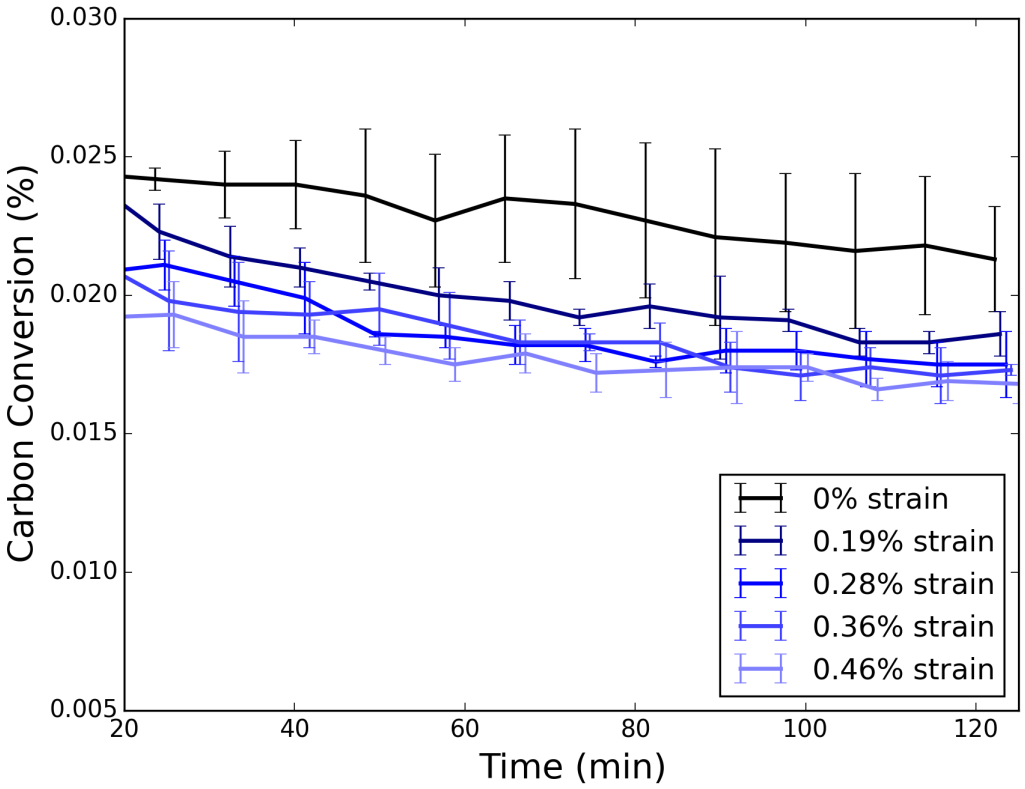

Figure 3: Percent carbon conversion and 95% confidence intervals

Reaction Step	0% ΔG_{TS}	0% ΔG_{rxn}	1% ΔG_{TS}	1% ΔG_{rxn}
$CO(g) \longrightarrow CO*$	0.50	-1.09	0.50	-1.08
$CO* + * \longrightarrow C* + O*$	1.52	+0.12	1.45	+0.03
$C* + H* \longrightarrow CH* + *$	1.19	+0.45	1.20	+0.50
$CH* + H* \longrightarrow CH_2* + *$	1.13	+0.65	1.14	+0.69
$CH_2* + H* \longrightarrow CH_3* + *$	0.56	+0.01	0.56	0.00
$CH_3* + H* \longrightarrow CH_4(g) + 2*$	0.99	-0.45	0.99	-0.46
$O* + H* \longrightarrow OH* + *$	0.91	+0.08	0.92	+0.12
$OH* + H* \longrightarrow H_2O(g) + 2*$	1.24	+0.33	1.24	+0.32

Table 2: Reaction energies for unstrained and 1% strained surfaces.

drogenation. For hydrogenation, the single barrier height can be computed as the energy difference between the lowest energy dissociated state and the highest energy transition state. While increased strain causes the CO dissociation barrier to decrease, it also causes the single hydrogenation barrier to increase by a similar amount. Note that these values assume that C* is completely hydrogenated to CH_4 before O* is hydrogenated; barrier values differ slightly if the order of C* and O* is changed, although the same trend can be observed.

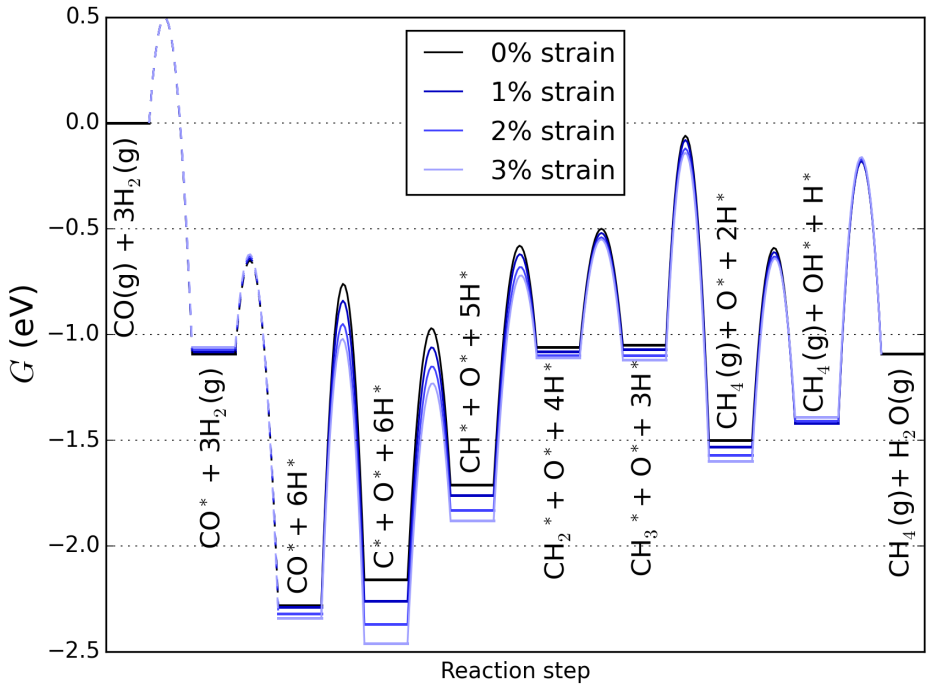

Figure 4: Free energy diagram for methanation on strained and unstrained Ni(211). As discussed in Section 2.3, barrier calculations were estimated using scaling relation data [14, 15, 16]. Barriers for CO adsorption and dissociative H_2 adsorption are estimated based on collision theory using a sticking probability of 1; using these values in appropriate rate equations gives an adsorption rate equal to that predicted by collision theory.

Reaction Step	2% ΔG_{TS}	2% ΔG_{rxn}	3% ΔG_{TS}	3% ΔG_{rxn}
$CO(g) + * \longrightarrow CO*$	0.50	-1.07	0.50	-1.06
$CO* + * \longrightarrow C* + O*$	1.37	-0.05	1.32	-0.12
$C* + H* \longrightarrow CH* + *$	1.22	+0.54	1.23	+0.58
$CH* + H* \longrightarrow CH_2* + *$	1.15	+0.73	1.16	+0.77
$CH_2* + H* \longrightarrow CH_3* + *$	0.56	0.00	0.56	0.00
$CH_3* + H* \longrightarrow CH_4(g) + 2*$	0.98	-0.46	0.98	-0.48
$O* + H* \longrightarrow OH* + *$	0.94	+0.16	0.96	+0.21
$OH* + H* \longrightarrow H_2O(g) + 2*$	1.24	+0.32	1.23	+0.29

Table 3: Reaction energies for 2% strained and 3% strained surfaces.

3.5 Discussion and Conclusions

The initial objective of this study was to design and construct a thermochemical reactor for CO methanation over a Ni catalyst subjected to an externally applied mechanical strain. The study was successful in accomplishing this goal, and we believe this is the first study to successfully combine an externally applied strain with a thermochemical catalytic reactor. Previous studies have typically used either electrochemical reactors or intrinsically strained core-shell nanoparticles

Strain	CO dissociation barrier (eV)	Hydrogenation barrier (eV)
0%	1.52	2.10
1%	1.45	2.18
2%	1.37	2.25
3%	1.32	2.33

Table 4: Barriers as a function of strain

or similar bimetallic systems. There were multiple challenges in the approach demonstrated in this study which had to be addressed in order to successfully carry out and measure the desired reaction. It is therefore significant in demonstrating another method in which the chemical properties of a system can be manipulated through purely mechanical means, which may lead to the development of novel low-cost catalyst materials.

While the present study was able to create a strain-induced change in reactivity, it ultimately found that the application of tensile strain to a Ni catalyst had a negative effect on the methanation reaction rate. This was the opposite of what had been suggested in previous computational literature.

The computational model used in previous literature was re-examined in order to address the apparent discrepancy between what is proposed by those works and what was observed in the present study. This re-examination was careful to consider the rate-determining behavior of hydrogenation steps as well as CO dissociation. Our results suggest that previous literature was correct in predicting that tensile strain would increase the rate at which CO dissociation occurred. Separate C* and O* adsorbates bind more strongly as strain increases, while the binding of CO* is relatively constant. This would be expected to lower the CO dissociation barrier according to the Bell-Evans-Polanyi principle. However, the same principle also predicts that barriers will increase for hydrogenating the separate C* and O* adsorbates. Our results suggest that the increased rate of C-O scission is more than offset by the decreased rate of hydrogenation and that the net effect is a decrease in the overall methanation rate.

4 Conflicts of interest

There are no conflicts of interest to declare.

5 Acknowledgments

Funding was provided by the Army Research Office through award W911NF-11-1-0353. Computations were undertaken at the Center for Computation & Visualization, Brown University.

6 References

[1] M. Mavrikakis, B. Hammer, and J. Nørskov, "Effect of Strain on the Reactivity of Metal Surfaces," *Phys. Rev. Lett.*, vol. 81, pp. 2819–2822, 1998.

[2] A. Khorshidi, J. Violet, J. Hashemi, and A. A. Peterson, "How strain can break the scaling realtions of catalysis," *Nature Catalysis*, vol. 1, pp. 263–268, 2018.

[3] J. Wu, P. Li, Y.-T. F. Pan, S. Warren, X. Yin, and H. Yang, "Surface lattice-engineered bimetallic nanoparticles and their catalytic properties.," *Chemical Society Reviews*, vol. 41, no. 24, pp. 8066–74, 2012.

[4] T. A. Maark and A. A. Peterson, "Understanding strain and ligand effects in hydrogen evolution over Pd(111) surfaces," *Journal of Physical Chemistry C*, vol. 118, no. 8, pp. 4275–4281, 2014.

[5] Q. Deng, M. Smetanin, and J. Weissmuller, "Mechanical modulation of reaction rates in electrocatalysis," *Journal of Catalysis*, vol. 309, pp. 351–361, 2014.

[6] Y. Yang, T. A. Maark, A. A. Peterson, and S. Kumar, "Elastic strain effects on catalysis of a PdCuSi metallic glass thin film," *Physical Chemistry Chemical Physics*, vol. 17, pp. 1746–1754, 2015.

[7] M. Du, L. Cui, Y. Cao, and A. J. Bard, "Mechanoelectrochemical Catalysis of the Effect of Elastic Strain on a Platinum Nanofilm for the ORR Exerted by a Shape Memory Alloy Substrate," *Journal of the American Chemical Society*, vol. 137, pp. 7397–7403, 2015.

[8] K. Yan, T. A. Maark, A. Khorshidi, V. A. Sethuraman, A. A. Peterson, and P. R. Guduru, "The influence of elastic strain on catalytic activity in the hydrogen evolution reaction," *Angewandte Chemie - International Edition*, vol. 55, no. 21, pp. 6175–6181, 2016.

[9] K. Yan, S. K. Kim, A. Khorshidi, P. R. Guduru, and A. A. Peterson, "High Elastic Strain Directly Tunes the Hydrogen Evolution Reaction on Tungsten Carbide," *Journal of Physical Chemistry C*, vol. 121, pp. 6177–6183, 2017.

[10] M. F. Francis and W. A. Curtin, "Mechanical work makes important contributions to surface chemistry at steps.," *Nature Communications*, vol. 6, p. 6261, 2015.

[11] A. H. Larsen, J. J. Mortensen, J. Blomqvist, I. E. Castelli, R. Christensen, M. Dułak, J. Friis, M. N. Groves, B. Hammer, C. Hargus, E. D. Hermes, P. C. Jennings, P. B. Jensen, J. Kermode, J. R. Kitchin, E. L. Kolsbjerg, J. Kubal, K. Kaasbjerg, S. Lysgaard, J. B. Maronsson, T. Maxson, T. Olsen, L. Pastewka, A. Peterson, C. Rostgaard, J. Schiøtz, O. Schütt, M. Strange, K. S. Thygesen, T. Vegge, L. Vilhelmsen, M. Walter, Z. Zeng, and K. W. Jacobsen, "The Atomic Simulation Environment—a python library for working with atoms," *Journal of Physics: Condensed Matter*, vol. 29, no. 27, p. 273002, 2017.

[12] B. Hammer, L. Hansen, and J. Nørskov, "Improved adsorption energetics within density-functional theory using revised Perdew-Burke-Ernzerhof functionals," *Physical Review B*, vol. 59, pp. 7413–7421, mar 1999.

[13] C. Broyden, "The Convergence of Single-Rank Methods," *Mathematics of Computation*, vol. 24, no. 110, pp. 365–382, 1970.

[14] S. Wang, V. Petzold, V. Tripkovic, J. Kleis, J. G. Howalt, E. Skúlason, E. M. Fernández, B. Hvolbæk, G. Jones, A. Toftelund, H. Falsig, M. Björketun, F. Studt, F. Abild-Pedersen, J. Rossmeisl, J. K. Nørskov, and T. Bligaard, "Universal transition state scaling relations for (de)hydrogenation over transition metals.," *Physical Chemistry Chemical Physics*, vol. 13, pp. 20760–5, dec 2011.

[15] S. Wang, B. Temel, J. Shen, G. Jones, L. C. Grabow, F. Studt, T. Bligaard, F. Abild-Pedersen, C. H. Christensen, and J. K. Nørskov, "Universal Bronsted-Evans-Polanyi relations for C-C, C-O, C-N, N-O, N-N, and O-O dissociation reactions," *Catalysis Letters*, vol. 141, no. 3, pp. 370–373, 2011.

[16] M. P. Andersson, F. Abild-Pedersen, I. N. Remediakis, T. Bligaard, G. Jones, J. Engbæk, O. Lytken, S. Horch, J. H. Nielsen, J. Sehested, J. R. Rostrup-Nielsen, J. K. Nørskov, and I. Chorkendorff, "Structure sensitivity of the methanation reaction: H_2-induced CO dissociation on nickel surfaces," *Journal of Catalysis*, vol. 255, no. 1, pp. 6–19, 2008.

[17] H. Bengaard, J. Nørskov, J. Sehested, B. Clausen, L. Nielsen, A. Molenbroek, and J. Rostrup-Nielsen, "Steam Reforming and Graphite Formation on Ni Catalysts," *Journal of Catalysis*, vol. 209, no. 2, pp. 365–384, 2002.

[18] M. P. Andersson, T. Bligaard, A. Kustov, K. E. Larsen, J. Greeley, T. Johannessen, C. H. Christensen, and J. K. Nørskov, "Toward computational screening in heterogeneous catalysis: Pareto-optimal methanation catalysts," *Journal of Catalysis*, vol. 239, no. 2, pp. 501–506, 2006.

[19] T. Bligaard, J. K. Nørskov, S. Dahl, J. Matthiesen, C. H. Christensen, and J. Sehested, "The Bronsted-Evans-Polanyi relation and the volcano curve in heterogeneous catalysis," *Journal of Catalysis*, vol. 224, no. 1, pp. 206–217, 2004.